Energy Reports xxx (xxxx) xxx

Contents lists available at ScienceDirect

Energy Reports

journal homepage: www.elsevier.com/locate/egyr

Research paper

Numerical analyses of concrete thermal energy storage systems: effect of the modules' arrangement

Luca Doretti [a,*], Francesca Martelletto [a], Simone Mancin [b]

[a] Department of Civil, Environmental and Architectural Engineering, University of Padova, Via Venezia, 1, Padova 35131, Italy
[b] Department of Management and Engineering, University of Padova, Stradella S. Nicola, 3, Vicenza 36100, Italy

ARTICLE INFO

Article history:
Received 27 April 2020
Received in revised form 19 June 2020
Accepted 3 July 2020
Available online xxxx

Keywords:
Sensible heat storage
Concrete module
Series and parallel
Performance optimization

ABSTRACT

This paper is focused on modularized concrete sensible thermal energy storage systems with thermal oil as heat transfer fluid; the thermal storage systems have been conceived to be integrated into a concentrated solar power plant. This work is mainly focused on the effect of the modules' arrangement on the overall performance of the thermal energy storage system. Series and parallel arrangements are investigated, to determine the most performant solutions in terms of exchanged thermal energy as a function of the main operating conditions: oil mass flow rate and pressure drop, both in heating and cooling phase. Two different boundary conditions are considered: adiabatic and diabatic external walls. The simulations are carried out using an extended version of a model proposed by the present authors for a single concrete block, that was validated with experimental data. The exchanged thermal energy, the oil mass flow rate, the pressure drops, and the duration of the process are changed to evaluate the storages under different operating conditions. The best thermal energy storage configuration is determined by a thermal energy assessment: it coincides with the first one that reaches the asymptotic values with the minimum number of elements. Furthermore, in the diabatic case, the loss heat flux toward the environment has a significant role and highlights the differences between charging and discharging phases, its presence contributed to a more aware choice of the most suitable and performant modularized system.

1. Introduction

It is a common opinion that energy production should involve sustainable and renewable resources and other technologies that can optimize the overall process. The thermal energy storage (TES) is one of the most attractive ways to improve concentrated solar power (CSP) plant performances (Gil et al., 2010; Medrano et al., 2010; Kuravi et al., 2013; Pelay et al., 2017), by meeting the energy peak demand during cloudy weather or overnight. In the charging or heating phase, the solar field heats the heat transfer fluid (HTF), which commonly flows inside pipes embedded in the TES. Then, it warms up the TES and stores energy by increasing its temperature. Conversely, during the discharging or cooling phase, the cold fluid is pumped through the TES to extract the thermal energy that will be employed in the power plant. In particular, concrete is widely used for TES construction because of its thermal, mechanical and affordable properties (Salomoni et al., 2014; Laing et al., 2006, 2009; Tamme et al., 2004).

This paper is focused on modularized concrete sensible TES systems and the most efficient modules' arrangement is investigated, both in the heating and cooling phase. Different series, parallel and mixed configurations are considered, and their performances are evaluated, combining the exchanged thermal energy, the mass flow rate and the pressure drops along with the system. Many studies about TES modularization have been conducted but a specific comparison of the stored energy amount and a focus on the series or parallel connection are still missing in the open literature.

Many types of TES modularization have been studied. Haller et al. (2009) reviewed different methods to characterize thermal stratification in energy storage, focusing on the methods that can be used to determine the ability to promote and maintain stratification. The thermal response of a multi-tank TES was studied by Cruickshank and Harrison (2011). The storage was assembled from three standard hot-water storage tanks which were connected in series or parallel configuration. The series ones reached high levels of temperature stratification during periods of rising temperatures and limited destratification during periods of falling temperature. This effect was not observed in the parallel one. Then, Dickinson et al. (2013) investigated the thermal behavior of

* Corresponding author.
E-mail address: luca.doretti@unipd.it (L. Doretti).

https://doi.org/10.1016/j.egyr.2020.07.002

Nomenclature

c	specific heat capacity [J kg^{-1} K^{-1}]
D	diameter [m]
e	roughness [m]
f	friction factor [-]
L	length [m]
$\dot{m}$	mass flow rate [kg s^{-1}]
m	mass [kg]
Nu	Nusselt number [-]
p	pressure [Pa]
q	heat flow rate [W]
R	thermal resistance [K W^{-1}]
Re	Reynolds number [-]
t	temperature [°C]
v	velocity [ms^{-1}]

Greek symbols

γ	interpolation coefficient [-]
Δ	difference [-]
ε	efficiency [-]
ρ	density [kg m^{-3}]
τ	time [s]

Subscript

amb	ambient
cnc	concrete
ext	external
in	inlet
ins	insulating layer
int	internal
loss	dissipated
m	mean value
oil	oil
out	outlet

Acronyms

CFD	Computational Fluid Dynamics
CSP	Concentrating Solar Power
HTF	Heat Transfer Fluid
PCM	Phase Change Material
S*P	Series*Parallel
TES	Thermal Energy Storage

a stratified tank when subjected to constant temperature charging and constant volume hourly draws. Charging in the series configuration was the most effective option, when combined with parallel draws, led to the mixing of unequal delivery temperatures from the tanks. Macias et al. (2018) examined soda lime silicate glass–graphite composites for use as a storage medium in a TES unit. A simple one-dimensional model for thermal conductivity was developed based on equivalent thermal circuits for series–parallel composite walls but without an optimization analysis. Venegas-Reyes et al. (2019) presented a parametric methodology to size stationary solar collector fields. The costs of the collector loop piping and the pumping power of different series–parallel arrays are considered. The optimal series–parallel array was determined by the assessment of the payback time. Vigneshwaran et al. (2019) developed a cost-effective concrete based TES system by performing experimental studies and numerical simulations. For evaluating the temperature variation along the length of the module, an object-oriented framework is adopted by implementing the theory of continuous stirred tank in series. Yongtai et al. (2019) designed a heat storage vacuum tube solar collector. The parallel and series–parallel solar air collector system prototype was designed and tested but without a focus on the best disposition.

Cimmino (2019) presented a semi-analytical method for the calculation of g-functions of bore fields with mixed arrangements of series and parallel connected boreholes. However, it was not possible to account for changes in flow direction within the bore field, which is expectable in seasonal storage systems. Rosato et al. (2019) investigated the performance of an Italian district heating network. The plant was based on the operation of solar thermal collectors connected to a double U-pipe vertical borehole TES. They analyzed also the connection type (series, parallel or mixed) and found out that for a given number of borehole TES, the series one was the most performant. Anyhow, they considered just a few elements in the simulation.

The TES systems that are based on Phase Change Materials (PCM) are also gaining attention because of their potential improvements. Keshavarz et al. (2010) studied a TES system, consisting of different PCMs arranged in series, from the irreversibility point of view, with charging and discharging processes occurring periodically. The number of PCMs and their arrangement influenced the irreversibility of the system. Amirifard et al. (2018) studied the integration of a solar pond with latent heat storage for performance stability. Two parallel and one series layouts were studied. The average efficiency of discharging time for the series layout showed a higher increase compared with the parallel one. A hybrid concentrator photovoltaic PCM system was developed by Emam and Ahmed (2018). The developed system included four different configurations of PCM heat sinks and nine different pattern arrangements of PCM. Increasing the number of parallel cavities led to a reduction in solar cell temperature. However, increasing series cavities had an unfavorable effect on the solar cell temperature. Shang et al. (2018) proposed modularized TES fabricated by encapsulating paraffin, thermally enhanced via copper or nickel foams, with epoxy resin. Theoretical and experimental validations revealed that the effective thermal conductivity was increased, and they also developed a series–parallel model to predict it. Besagni and Croci (2019) proposed a pilot-scale PCM storage, to be coupled with solar-assisted heat pumps. The storage system was operated considering series and parallel heat exchanger configurations and implementing a broad set of boundary conditions, to test the storage unit under relevant operating conditions. Rezaei et al. (2020) presented a design methodology for a high-temperature latent heat TES unit, employing metal PCM. They assessed that the in-series or in-parallel arrangement of multiple units into a complete system provides higher performances, but they did not study which layout gave the best result. Huang et al. (2020) proposed a system using a PCM as a TES unit combined with a water tank for solar heating systems. The series system showed an enhancement of the solar fraction compared with a single water tank system and with a water tank-PCM unit parallel system. However, they did not multiple element configurations.

Concrete TES systems have been studied mainly for CSP integrations. A new type of TES for CSP plants was presented by Bergan and Greiner (2014). The energy storage medium is concrete with high thermal conductivity. Heat is transported by the HTF which flows through the steel pipe. The flow through the modular system is arranged in parallel and series but without a specific investigation of the best configuration. Concrete was also studied for TES integration in CSP plants by Wu et al. (2014). The discharging performance of four concrete structures is studied.

Please cite this article as: L. Doretti, F. Martelletto and S. Mancin, Numerical analyses of concrete thermal energy storage systems: effect of the modules' arrangement. Energy Reports (2020), https://doi.org/10.1016/j.egyr.2020.07.002.

The packed-bed gives the best discharging performance, followed by the rod-bundle structure, the parallel-plate structure, and the channel-embedded structure. Hoivik et al. (2019) studied a TES based on concrete modular system design with steel pipe heat exchangers. A heat exchanger design using thermal elements arranged in series and parallel was developed. Multiple thermal elements were stacked inside a steel frame, and the elements were connected through pipes. The pipes in each element were configured so that the HTF flows in and out of one element through two parallel U-shaped pipes. However, the authors did not focus on finding the most efficient series/parallel configuration. Suárez et al. (2020) developed a simplified zero-dimensional model of a passive sensible TES system for application in CSP plants, using concrete as a storage medium and thermal oil as HTF. The authors used a correction function determined through a set of Computational Fluid Dynamics (CFD) numerical simulations and they did not investigate the effect of series/parallel disposition of the elements. Roy et al. (2020) studied a sensible TES made of concrete and water as HTF. The computational work was carried out using Comsol Multiphysics software, with a specific focus on the exergy factor, but without consideration of the possible modularized arrangements.

The present work follows a previous study already published by Doretti et al. (2019). The paper presented a simple lumped capacitance-based computing model for a single concrete module that is recalled in the following model description.

2. Model description

The model proposed by Doretti et al. (2019) aimed at developing a computational tool to predict the behavior of a single concrete storage module. It allowed for the real-time simulation of the general TES module's parameters during the operation of the entire system. The main parameter describing the TES is the stored or released thermal energy from or to the HTF. So, the model was meant to compute the transferred energy over time, and the related HTF temperature at the outlet of the module. To validate the developed model, a suitable set of experimental tests was selected, the agreement between numerical simulations and tests was very good (Doretti et al., 2019).

The storage element consists of a stainless steel AISI 316 tube embedded into the concrete matrix in a 4-passages configuration. The module is 3 m long while the tube has an inner diameter equal to 14 mm and an outer diameter of 16 mm, the total tube length is 12 m. It has a square cross-section parallelepiped (0.2×0.2 m), with a total weight of around 290 kg, as can be seen in Fig. 1. Paratherm™ NF mineral oil (Paratherm NF Bulletin) was chosen as HTF. The modules were covered with two insulating layers, one made of ceramic wool and the other by Rockwool, to reduce the convective heat losses to the surroundings.

The proposed model schematized the concrete storage module as a cylinder with an equivalent diameter. The storage module was considered as 4 sub-units arranged in series. In this way, the basic element assumes the well-known geometry, often described as "washer", in which the tube is placed in the cylinder center; in the specific case, each of 4 elements has 2 adiabatic sides (toward the adjacent elements), and 2 diabatic sides (toward the external insulating layers). All the simplified simulation models are based on the well-known lumped capacitance method with other additional assumptions (Doretti et al., 2019).

2.1. Governing equations

When combining the internal (A) and external (B) section calculations and considering the 4 basic elements arranged in series that constitute the entire TES module, the heat flux balance for the entire TES element for the heating and cooling phase can be written.

Heating/charging phase energy balance (Fig. 2, left-hand side schematic):

$$q_{cnc,A} = q_{oil,A} \quad q_{cnc,B} = q_{oil,B} - q_{ins} - q_{loss} \tag{1, 2}$$

$$q_{cnc} = q_{cnc,A} + q_{cnc,B} = q_{oil,A} + q_{oil,B} - q_{ins} - q_{loss} \tag{3}$$

Cooling/discharging phase energy balance (Fig. 2, right-hand side schematic):

$$q_{cnc,A} = q_{oil,A} \quad q_{cnc,B} = q_{oil,B} - q_{ins} + q_{loss} \tag{4, 5}$$

$$q_{cnc} = q_{cnc,A} + q_{cnc,B} = q_{oil,A} + q_{oil,B} - q_{ins} + q_{loss} \tag{6}$$

In this way, after an iterative procedure on heat fluxes and temperatures, the internal energy variation of concrete TES and, consequently, the new value of TES element temperature can be obtained at each time-step:

$$\Delta t_{cnc} = \frac{q_{cnc}}{m_{cnc} c_{cnc}} \cdot \Delta\tau = \left| t_{cnc,\tau+\Delta\tau} - t_{cnc,\tau} \right| \tag{7, 8}$$

$$t_{cnc,\tau+\Delta\tau} = t_{cnc,\tau} \pm \Delta t_{cnc} \tag{9}$$

with the sign (+) for heating (the concrete temperature is increasing) and sign (−) for cooling (the concrete temperature is decreasing). The HTF Nusselt number is considered equal to 3.66 in the laminar zone, while it is estimated with the well-known Dittus–Boelter semi-empirical correlation (Dittus and Boelter, 1930) in the turbulent zone, and interpolated as reported by Gnielinski (2013) in the transition zone:

$$Nu = (1 - \gamma) \cdot Nu_{lam,2300} + \gamma \cdot Nu_{turb,4000} \tag{10}$$

with:

$$\gamma = \frac{Re - 2300}{4000 - 2300} \tag{11}$$

where $Nu_{lam,2300}$ is the Nusselt number at the end of the laminar zone (Re = 2300) and $Nu_{turb,4000}$ is the Nusselt number at the beginning of the turbulent zone (Re = 4000).

The heat flux equations are here reported for the two different processes: thus, referring to heating/charging process (in which the oil heats the concrete TES), and in the case of cooling/discharging (in which the concrete heats the oil mass flux) in which the absolute value has to be used.

The heat flux between oil and concrete for the internal section (called "A", from the oil to the TES core), considering the TES module (i.e the sum of the 4 sub-units), is defined as:

$$q_{oil,A} = \left| \frac{t_{oil,m} - t_{cnc}}{2R_{int}} \right| \tag{12}$$

section A is geometrically equal to the B one, each section has half of the entire area, so the overall thermal resistance is multiplied by a factor 2.

The heat flux between oil and concrete for the external section (called "B", from the oil to the TES boundaries), considering the TES module (the sum of the 4 sub-units), is given by:

$$q_{oil,B} = \left| \frac{t_{oil,m} - t_{cnc,ext}}{2R_{int}} \right| \tag{13}$$

while the heat flux between concrete and environment is:

$$q_{loss} = \frac{t_{cnc,ext} - t_{amb}}{R_{ext}} \tag{14}$$

Please cite this article as: L. Doretti, F. Martelletto and S. Mancin, Numerical analyses of concrete thermal energy storage systems: effect of the modules' arrangement. Energy Reports (2020), https://doi.org/10.1016/j.egyr.2020.07.002.

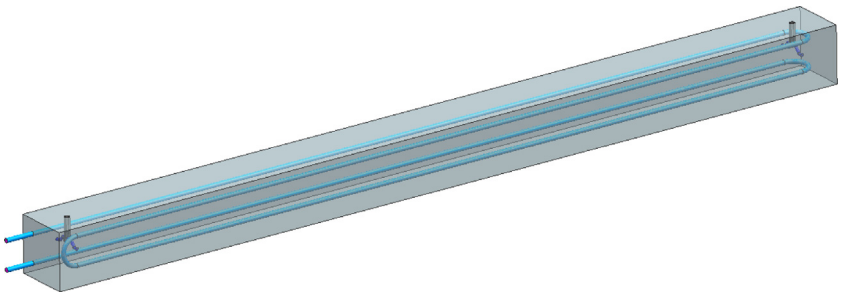

Fig. 1. Concrete module and piping 3D sketch.

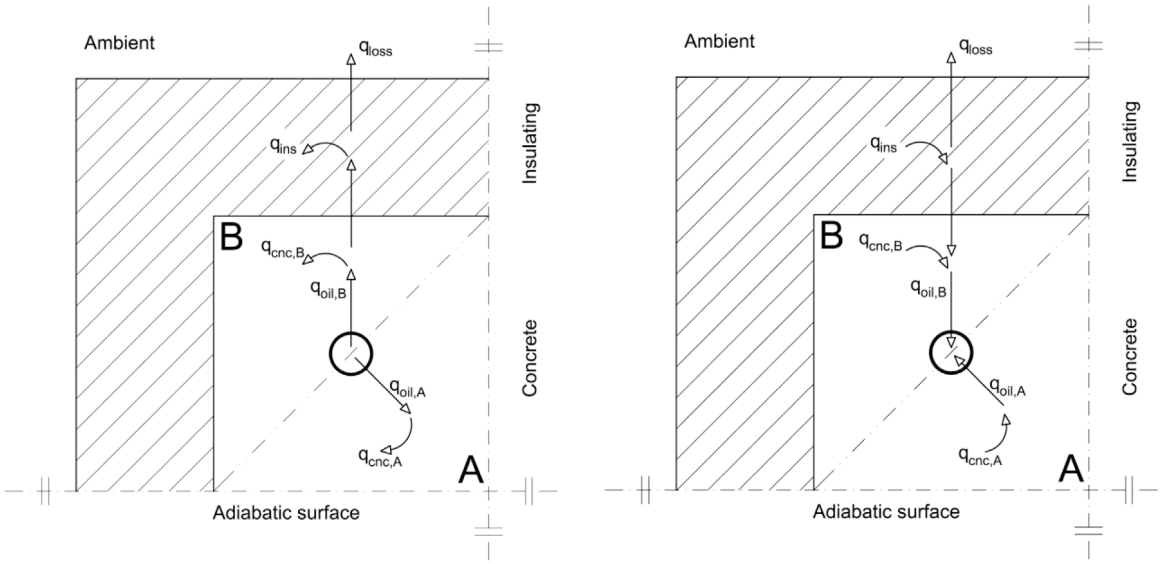

Fig. 2. Heat fluxes scheme for heating (left) and cooling (right) test.

Table 1
Energy and thermal efficiency comparison between 2 blocks in series and parallel in charging phase.

Configuration [–]	Energy 1st block [MJ]	Energy 2nd block [MJ]	Total energy [MJ]	Efficiency [%]	Pressure drop [bar]
Single module	44.42	–	44.42	98.58	0.22
2 modules in series	44.42	43.99	88.41	98.11	0.44
2 modules in parallel	43.98	43.98	87.96	97.61	0.11

Table 2
Energy and thermal efficiency comparison between 2 blocks in series and parallel in discharging phase.

Configuration [–]	Energy 1st block [MJ]	Energy 2nd block [MJ]	Total energy [MJ]	Efficiency [%]	Pressure drop [bar]
Single module	44.11	–	44.11	97.92	0.21
2 modules in series	44.11	43.49	87.60	97.20	0.42
2 modules in parallel	43.31	43.31	86.62	96.12	0.11

This loss heat flux will be considered only in the second part of the analyses, while in the first considerations a quasi-infinite external thermal resistance $R_{ext} = \infty$, will be considered (i.e. adiabatic conditions).

The concrete external temperature can be estimated as:

$$t_{cnc,ext} = t_{oil,m} \pm \frac{q_{oil}}{R_{int}} = t_{oil,m} \pm \frac{q_{oil,A} + q_{oil,B}}{R_{int}} \quad (15)$$

with the sign (−) for heating, and sign (+) for cooling processes. The insulating temperatures are also calculated.

The internal energy stored in insulating layers due to their mean temperature variations is given by:

$$q_{ins1} = \frac{m_{ins1} c_{ins1} \Delta t_{ins1}}{\Delta \tau} \quad q_{ins2} = \frac{m_{ins2} c_{ins2} \Delta t_{ins2}}{\Delta \tau} \quad (16, 17)$$

$$q_{ins} = q_{ins1} + q_{ins2} \quad t_{oil,out} = t_{oil,in} \pm \frac{q_{oil}}{\dot{m}_{oil} \cdot c_{oil}} \quad (18, 19)$$

with (−) for charging (outlet oil temperature is lower than the inlet one) and (+) for discharging phase (outlet oil temperature is higher than the inlet one).

As described before, the model was developed for a single concrete module, but the present work aims to analyze the performance of a modular system composed of several elements arranged in series and parallel arrays. The elements arranged in parallel have all the same behavior, so these subdivisions are simply obtained by dividing the total oil mass flow rate by the number of parallel elements. All the calculations are then

Please cite this article as: L. Doretti, F. Martelletto and S. Mancin, Numerical analyses of concrete thermal energy storage systems: effect of the modules' arrangement. Energy Reports (2020), https://doi.org/10.1016/j.egyr.2020.07.002.

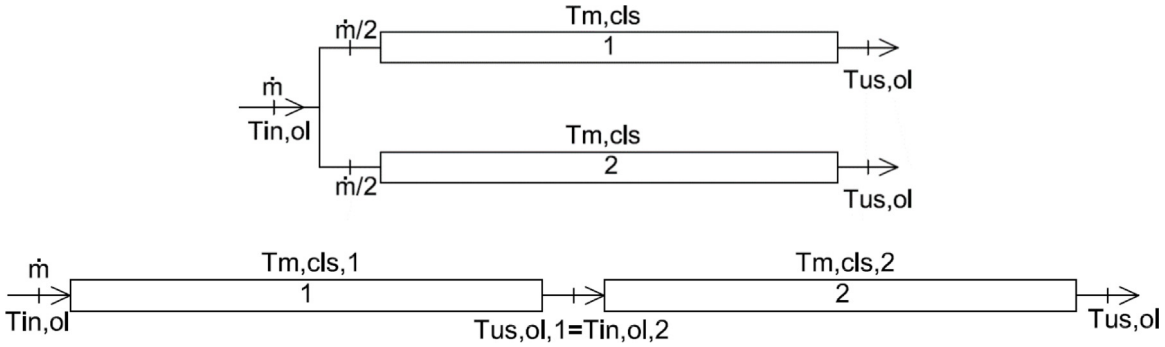

Fig. 3. Parallel (top) and series (bottom) disposition of two representative elements.

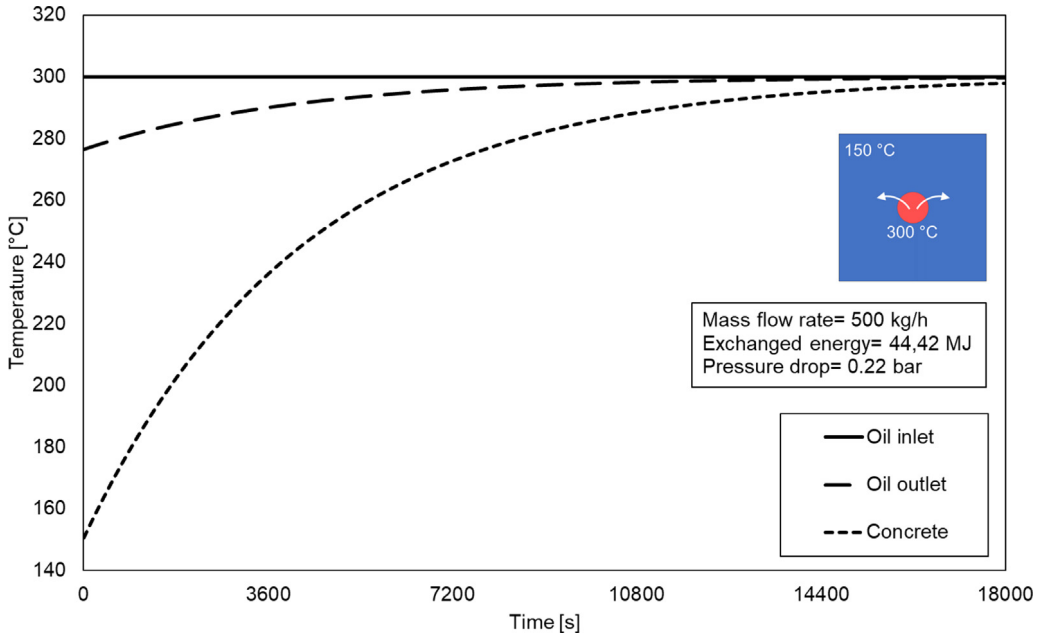

Fig. 4. Mean concrete and oil inlet and outlet temperature of a single element in charging.

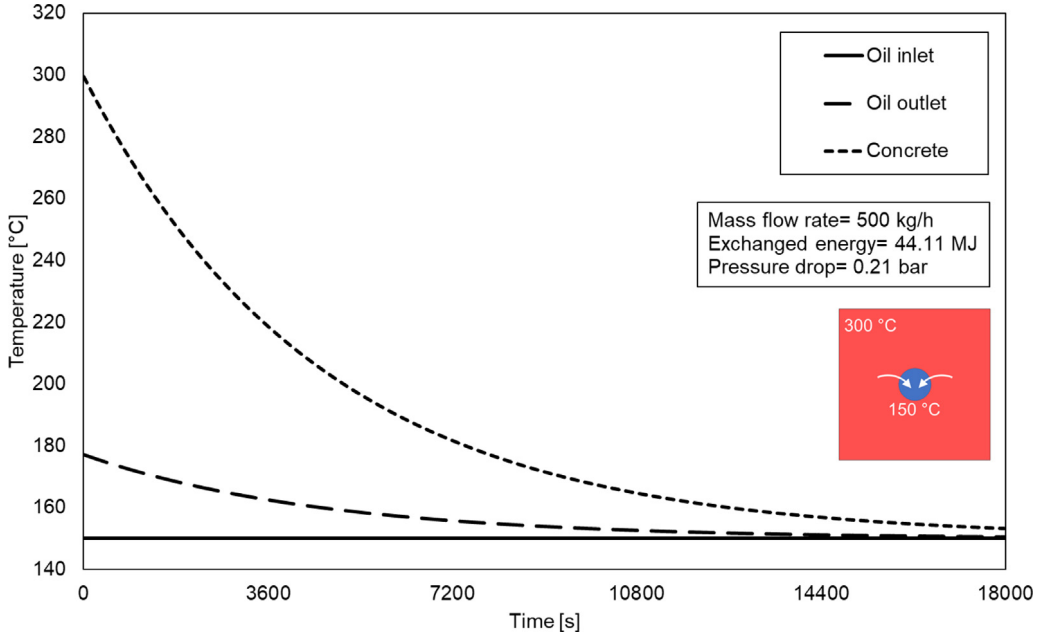

Fig. 5. Mean concrete and oil inlet and outlet temperature of a single element in discharging.

Please cite this article as: L. Doretti, F. Martelletto and S. Mancin, Numerical analyses of concrete thermal energy storage systems: effect of the modules' arrangement. Energy Reports (2020), https://doi.org/10.1016/j.egyr.2020.07.002.

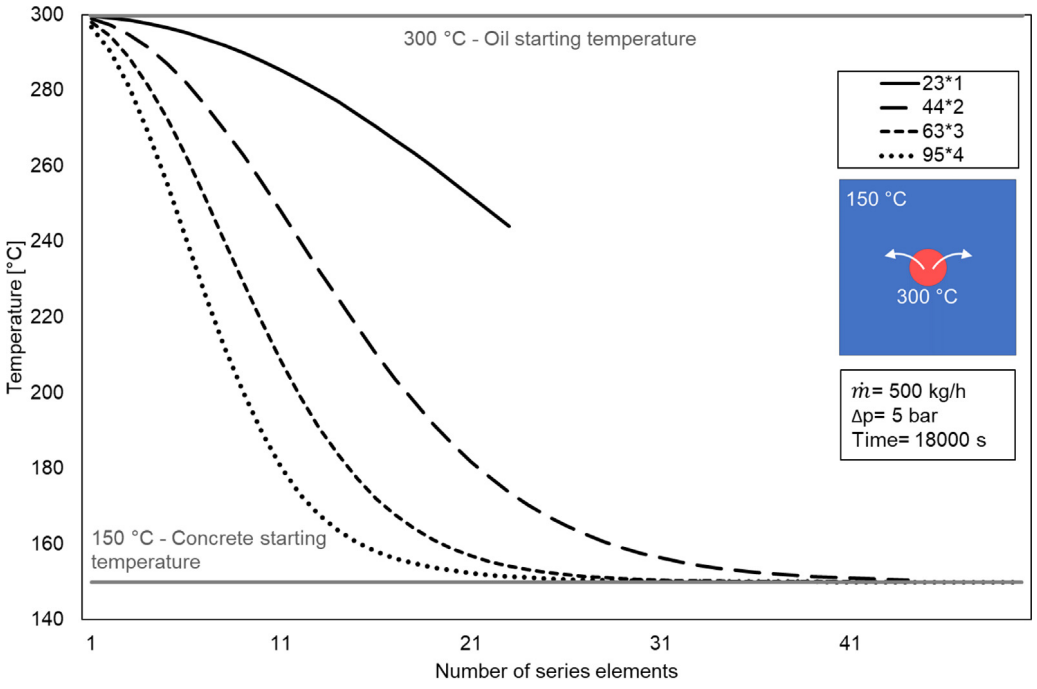

(a)

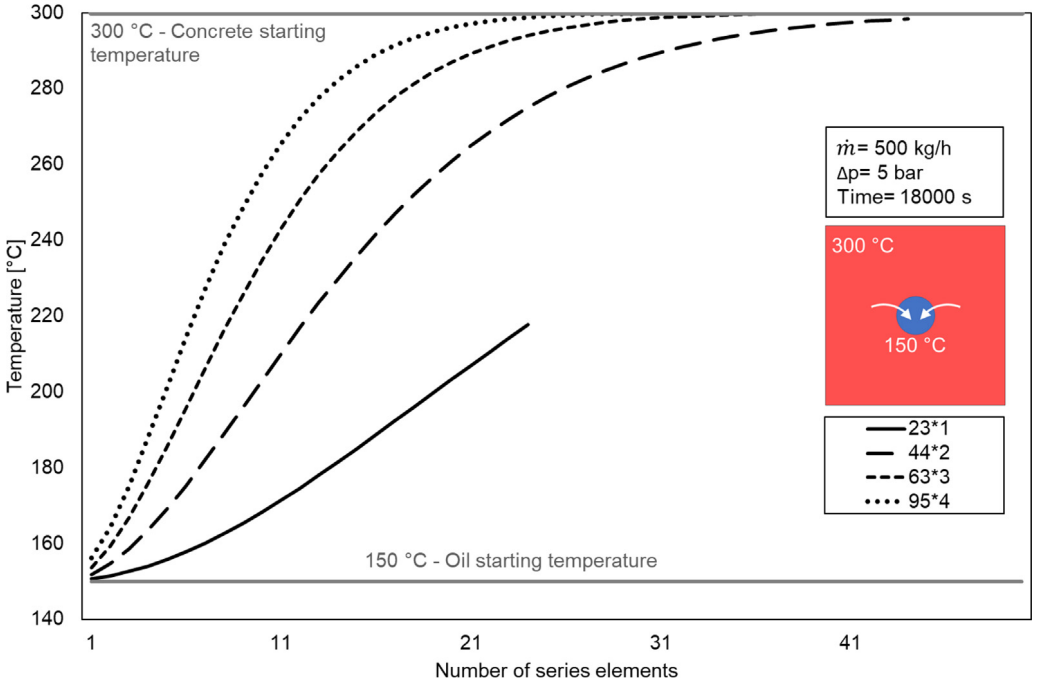

(b)

Fig. 6. Adiabatic analysis: oil temperature at the end of the simulation in charging (a) and discharging (b) for different configurations.

performed for a single element, then the total amount of energy is calculated by multiplying the resulted heat fluxes by the number of parallel elements.

Differently, the elements arranged in series present different working performances one from each other, the outlet oil of an element becomes the inlet of the following one. So, the oil temperature changes along with the series array and the code needed to be adapted to this configuration.

Mixed arrangements (with a variable number of branches and a different number of series elements) consider both the described procedure for series and parallel, in order to estimate their performance. The parallel and series arrangements of the elements is reported in Fig. 3 for two modules, as a clarifying scheme. The different temperatures and oil mass flow rate are also reported.

3. Pressure drops calculation

In order to identify the best option between series, parallel and mixed configurations in terms of overall performance, the

Please cite this article as: L. Doretti, F. Martelletto and S. Mancin, Numerical analyses of concrete thermal energy storage systems: effect of the modules' arrangement. Energy Reports (2020), https://doi.org/10.1016/j.egyr.2020.07.002.

thermal energy is not enough, and the analysis needs to consider also the related pressure drops. As expected, for the same amount of inlet oil mass flow rate, their value remarkably varies when passing from a pure parallel configuration to a pure series.

The pressure drops are a function of the friction factor, which depends on the laminar or turbulent flow. The HTF flows inside circular pipes, so the following equations are used:

- In laminar flow:

$$f = \frac{64}{Re} \tag{20}$$

- in turbulent flow, the well-known implicit Colebrook–White equation is implemented:

$$\frac{1}{\sqrt{f}} = -2\log\left(\frac{e}{3.7\,D_{int}} + \frac{2.51}{Re\sqrt{f}}\right) \tag{21}$$

The pressure drops are calculated by:

$$\Delta p = f\frac{L}{D}\rho\frac{v^2}{2} \tag{22}$$

4. Numerical simulations

All the numerical simulations presented in the following paragraphs are performed with the described code which in addition includes the possibility to estimate the performance of any different multiple module arrangements. The first part of the analyses considers the concrete blocks with adiabatic external surfaces. Then, the heat loss is introduced and a comparison with the adiabatic results is finally presented.

4.1. Adiabatic external boundaries

The first simulations consider adiabatic concrete surfaces. This condition is obtained by inserting a nearly-zero ambient heat transfer coefficient. In this way, the heat loss is equal to zero, so the exchanged heat fluxes are the ones related to concrete, oil and insulating material.

4.1.1. Single element simulations

A preliminary simulation with just one concrete block is conducted, both in the charging and discharging phase. The input parameters are chosen by referring to a compatible TES system in a CSP plant. So, in the charging phase the initial concrete temperature is set at 150 °C, the inlet oil temperature at 300 °C, the oil mass flow rate at 500 kg/h and the simulation time at 18000 s (5 h). The number of hours in which the solar energy overcomes the production request coincides with the loading time of the TES system. It varies concerning the latitude, the season and the industrialization level of the country in which the CSP plant is settled, so a simulation time of 5 h could be a reasonable value (Kuravi et al., 2013; Achkari and El Fadar, 2020; Herrmann and Kearney, 2002; Rodat et al., 2015; Zhang et al., 2013).

During the discharging phase, instead, the inlet oil temperature is set at 150 °C and the concrete one at 300 °C, while all the other parameters (e.g. oil mass flow rate and simulation time) keep the same values (Rodat et al., 2015; Achkari and El Fadar, 2020; Cocco et al., 2016; Rodríguez et al., 2016).

In this configuration, the thermal energy exchanged by oil and concrete is about 44 MJ, with a pressure drop of 0.2 bar, as reported in Figs. 4 and 5. During the simulation, the outlet oil and concrete temperature progressively get closer to the inlet oil temperature, with an asymptotic trend. This means that the energy exchanged by the two materials is very high at the beginning of the simulation, because of a high-temperature difference between oil and concrete and then decreases as the concrete temperature approaches the oil one.

Table 3
Thermal energy with 500 kg/h of mass flow rate and 2.5 bar of pressure drop for adiabatic (A) and diabatic (D) boundary.

Total blocks	Series	Parallel	Discharging		Charging	
[-]	[-]	[-]	[MJ]		[MJ]	
			A	D	A	D
11	11	1	470	403	453	431
44	22	2	1001	917	1037	1045
96	32	3	1090	1019	1091	1118
176	44	4	1091	1022	1091	1119
375	75	5	1091	1022	1091	1119
480	80	6	1091	1022	1091	1119
595	85	7	1091	1022	1091	1119
688	86	8	1091	1022	1091	1119

Table 4
Thermal energy with 500 kg/h of mass flow rate and 5 bar of pressure drop for adiabatic (A) and diabatic (D) boundary.

Total blocks	Series	Parallel	Discharging		Charging	
[-]	[-]	[-]	[MJ]		[MJ]	
			A	D	A	D
23	23	1	778	689	801	780
88	44	2	1089	1018	1091	1117
189	63	3	1091	1022	1091	1119
380	95	4	1091	1022	1091	1119
775	155	5	1091	1022	1091	1119
960	160	6	1091	1022	1091	1119
1155	165	7	1091	1022	1091	1119
1360	170	8	1091	1022	1091	1119

When more elements are put in series or parallel, with the same total oil mass flow rate, the exchanged thermal energy increases, but the increase is not proportional to the number of elements. In Tables 1 and 2 the comparisons between two elements in series and parallel, in charging and discharging phase respectively, are reported. If a second element is put in series to a previous one, the thermal energy increases, but that exchanged in the second block is lower than the one in the first block. This is due to the lower inlet oil temperature.

Besides, pressure drops also increase. If the two blocks are arranged in parallel, the total energy also increases, but it is lower than the one estimated for the series. Each block exchanges less because of the lower oil mass flow rate which leads to lower pressure drops.

In Tables 1 and 2, the thermal efficiency is also reported. It is calculated as the ratio between the value of the thermal energy stored in the TES and the maximum theoretical value, referred to inlet oil temperature. More details about the efficiency calculation are reported in Doretti et al. (2019). The efficiency is higher for a single block than for two elements. The series combination, also, achieves higher efficiencies, in both charging and discharging stages. However, the values are very similar for the three configurations, so the main difference is represented by the thermal energy amount, which is very different passing by one to two concrete blocks.

These considerations highlight the need of a more comprehensive analysis, in order to investigate the performances of more complex configurations, trying to identify a rationale best configuration for given operating conditions.

4.1.2. Thermal energy at a variable number of elements

The performance of different configurations was assessed at different operating conditions. The simulations started by keeping

Please cite this article as: L. Doretti, F. Martelletto and S. Mancin, Numerical analyses of concrete thermal energy storage systems: effect of the modules' arrangement. Energy Reports (2020), https://doi.org/10.1016/j.egyr.2020.07.002.

Table 5
Thermal energy with 500 kg/h mass flow rate and 10 bar pressure drop for adiabatic (A) and diabatic (D) boundary.

Total blocks	Series	Parallel	Discharging		Charging	
[-]	[-]	[-]	[MJ]		[MJ]	
			A	D	A	D
47	47	1	938	938	1057	1069
176	88	2	1022	1022	1091	1119
369	123	3	1022	1022	1091	1119
800	200	4	1022	1022	1091	1119
1550	310	5	1022	1022	1091	1119
1920	320	6	1022	1022	1091	1119
2289	327	7	1022	1022	1091	1119
2640	330	8	1022	1022	1091	1119

Table 6
Thermal energy with 250 kg/h of mass flow rate and 5 bar of pressure drop for adiabatic (A) and diabatic (D) boundary.

Total blocks	Series	Parallel	Discharging		Charging	
[-]	[-]	[-]	[MJ]		[MJ]	
			A	D	A	D
88	88	1	546	511	546	559
400	200	2	546	511	546	559
960	320	3	546	511	546	559
1320	330	4	546	511	546	559
1700	340	5	546	511	546	559
2082	347	6	546	511	546	559
2450	350	7	546	511	546	559
2816	352	8	546	511	546	559

Table 7
Thermal energy with 1000 kg/h of mass flow rate and 5 bar of pressure drop for adiabatic (A) and diabatic (D) boundary.

Total blocks	Series	Parallel	Discharging		Charging	
[-]	[-]	[-]	[MJ]		[MJ]	
			A	D	A	D
6	6	1	262	219	265	250
24	12	2	941	807	977	931
51	17	3	1599	1422	1691	1656
88	22	4	2003	1834	2107	2090
135	27	5	2149	2000	2170	2216
192	32	6	2179	2039	2182	2235
252	36	7	2183	2044	2183	2237
360	45	8	2183	2044	2183	2237

constant the initial concrete and oil temperatures, the total time and the total oil mass flow rate and then, for each number of branches (from 1 to 8), the number of elements arranged in series that lead to a target pressure drop was calculated. Finally, for each combination, the exchanged thermal energy was estimated. The results are listed in Tables 3–7.

For an oil mass flow rate of 500 kg/h and a target pressure drop of 2.5 bar, the combinations Series*Parallel (S*P) 11*1, 22*2, 32*3, etc. were obtained (Table 3). It means that with a mass flow rate of 500 kg/h and 3 branches, each branch needs 32 elements in series to get an overall pressure drop of 2.5 bar, with a total number of 96 elements. With a lower number of branches, the mass flow rate for each branch is higher, so the number of elements in series to reach the target pressure drop is lower (i.e. 22*2). The thermal energy during both charging and discharging phase was hence calculated. Table 3 also demonstrates that the total energy increases with the number of branches, because the total number of elements also increases (the elements numbers are valid both for adiabatic and diabatic boundary), but then it reaches an asymptotic value (for 3 branches), when the number of branches is increased, even if a higher number of elements is involved, the thermal energy remains almost the same, meaning that these configurations are not optimized.

When increasing the target pressure drop to 5 bar (Table 4), the resulted combinations, for a given number of branches, exhibit more modules arranged in series because of the greater amount of available pressure drop. The firsts were (S*P) 23*1, 44*2, 63*3 and so on. As already stated, by increasing the number of branches, the thermal energy also rises until the same asymptotic value of the previous simulations. However, in this case, the maximum value is obtained for lower parallel subdivisions (in particular, for 2 branches) because the number elements in series for each branch is higher. If the target pressure drop is brought to 10 bar (Table 5), the number of series elements for each branch increases accordingly, and the asymptotic thermal energy value is reached for 2 branches again.

Further considerations can be made by varying the oil mass flow rate, considering 250, 500 and 1000 kg/h, in Tables 6, 4 and 7, respectively, while keeping constant the value of the pressure drop at 5 bar. The asymptotic value is reached at lower number of branches for lower mass flow rate; in fact, at 250 kg/h it is achieved with the first combination yet, while with 1000 kg/h at 6 branches. In any case, the asymptotic thermal energy value is different for the three simulations, because it increases with the inlet oil mass flow rate.

This preliminary analysis allowed to understand the effect of the oil mass flow rate and pressure drop on the performance of different arrangements of concrete modules in complex TES systems. Besides, in order to understand the specific underlining heat transfer behavior of these systems in their charging and discharging phases, a more detailed analysis must be done. However, it is unfeasible to study in detail all the operating conditions presented before, thus a typical set of parameters for the HTF was considered (Rodat et al., 2015; Achkari and El Fadar, 2020; Cocco et al., 2016; Rodríguez et al., 2016). In particular, in the next paragraphs, the analysis was carried out by keeping constant the oil mass flow rate at 500 kg/h, as also reported in Rodat et al. (2015), Giannuzzi et al. (2017), while the maximum allowable oil pressure drops were limited to 5 bar, that can be considered a consistent value for a centrifugal pump available in the market.

4.1.3. Oil and concrete temperatures along the series

The detailed analysis can start from one of the most meaningful parameters, the oil temperature profiles through the series of the concrete modules for the different parallel configurations, in the case of adiabatic boundary conditions. The profiles relative to the first four modules arrangements (23*1, 44*2, 63*3 and 95*4), at the end of the process (5 h) at a mass flow rate of 500 kg/h and imposing the pressure drop at 5 bar, were plotted, both during charging (Fig. 6a) and discharging (Fig. 6b) phases. The profiles start at the inlet oil temperature and progressively approach the concrete one module by module, with a clear asymptotic trend. It is interesting to point out that the first configuration (23*1, pure series) does not reach the asymptote because the number of elements is limited by the allowable pressure drop. The second one (44*2) reaches the asymptotic value both for temperature and thermal energy (see Table 4): it is the first configuration that exchanges the maximum amount of thermal energy. All the other combinations also reach the asymptotic values, both for temperature and thermal energy (Table 4), but they employ a larger number of elements, becoming more expensive solutions without storing a greater amount of energy, which remains almost the same, as listed in Table 4.

Please cite this article as: L. Doretti, F. Martelletto and S. Mancin, Numerical analyses of concrete thermal energy storage systems: effect of the modules' arrangement. Energy Reports (2020), https://doi.org/10.1016/j.egyr.2020.07.002.

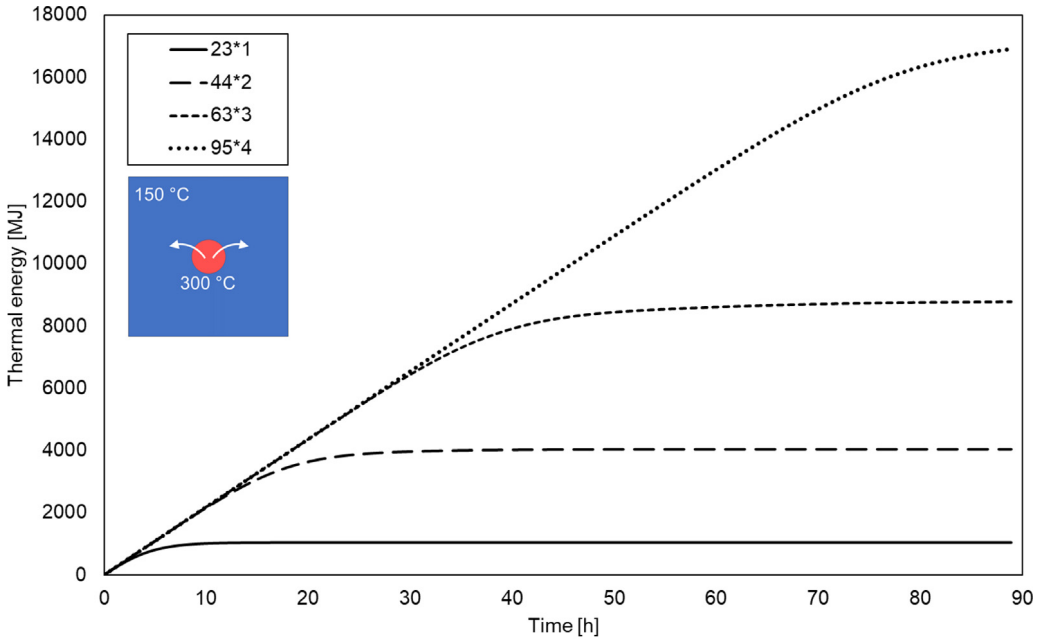

(a)

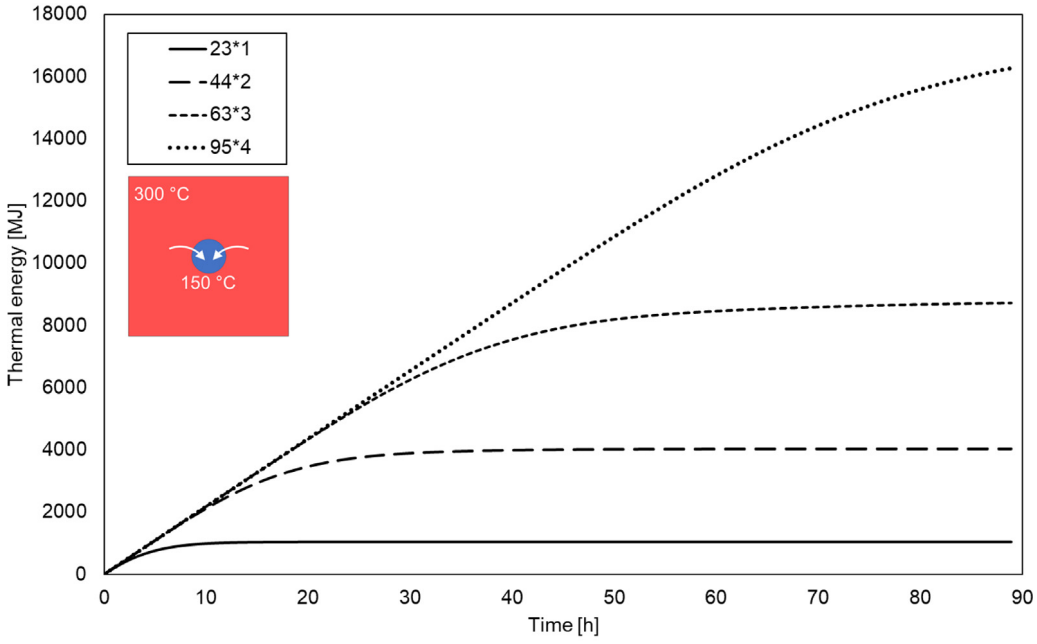

(b)

Fig. 7. Adiabatic analysis: energy for different configurations at constant mass flow rate (500 kg/h) and pressure drop (5 bar) in charging (a) and in discharging (b).

4.1.4. Thermal energy over time

The stored thermal energy over time allows for a more comprehensive understanding of the behavior of the different modules' configurations. In the previous analyses, the simulation time was always set to 5 h, which recalls a value of working hours for a typical CSP, that hardly can be extended to 6–8 h (at relatively high solar radiation). When the working time is increased, the selected configurations show interesting results, all the charging and discharging curves (Fig. 7a and 7b) present similar behavior because the temperature difference between oil and concrete and the other variables are set to equal values. In fact, the thermal energy profile of all the different combinations, at first linearly increases with time, then it approaches its specific asymptotic value, which depends upon the total number of elements and it is reached in a relative high time.

Considering a typical daily cycle for a CSP plant, the charging and discharging phases last in 6–8 h, thus, the first configuration 23*1 has almost achieved its asymptotic value yet; differently, all the other configurations are still in the linear zone, storing higher values of thermal energy. This is further proof that the second combination (44*2) is the optimal one (for the set simulation time) because it gets the same thermal energy of 63*3 and 95*4, but with fewer concrete blocks. With different simulation time, different optimal combination will be obtained.

Please cite this article as: L. Doretti, F. Martelletto and S. Mancin, Numerical analyses of concrete thermal energy storage systems: effect of the modules' arrangement. Energy Reports (2020), https://doi.org/10.1016/j.egyr.2020.07.002.

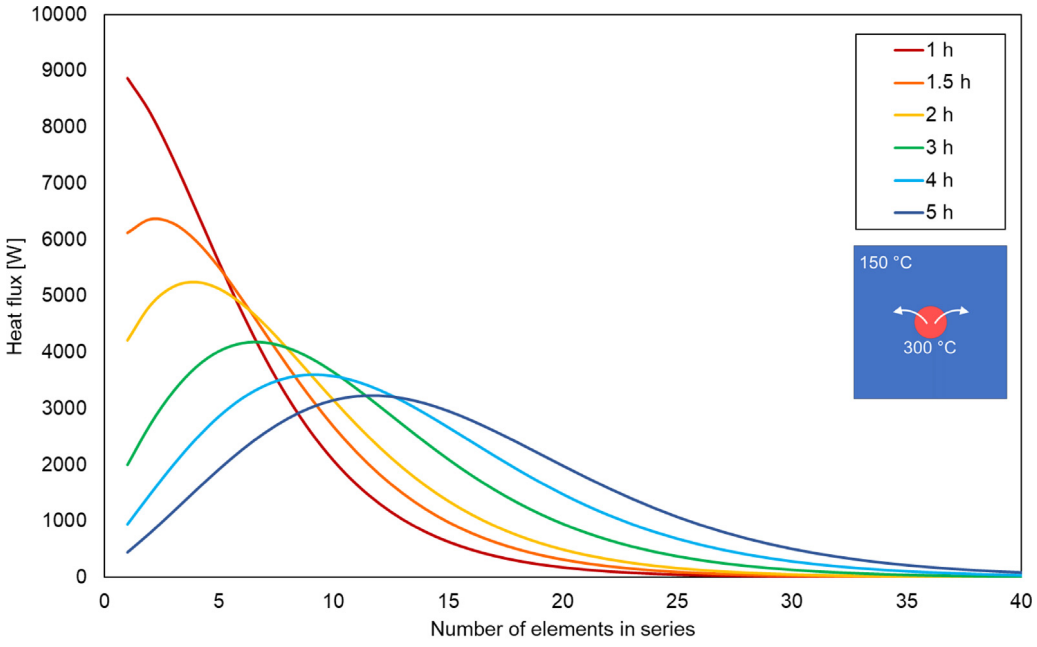

(a)

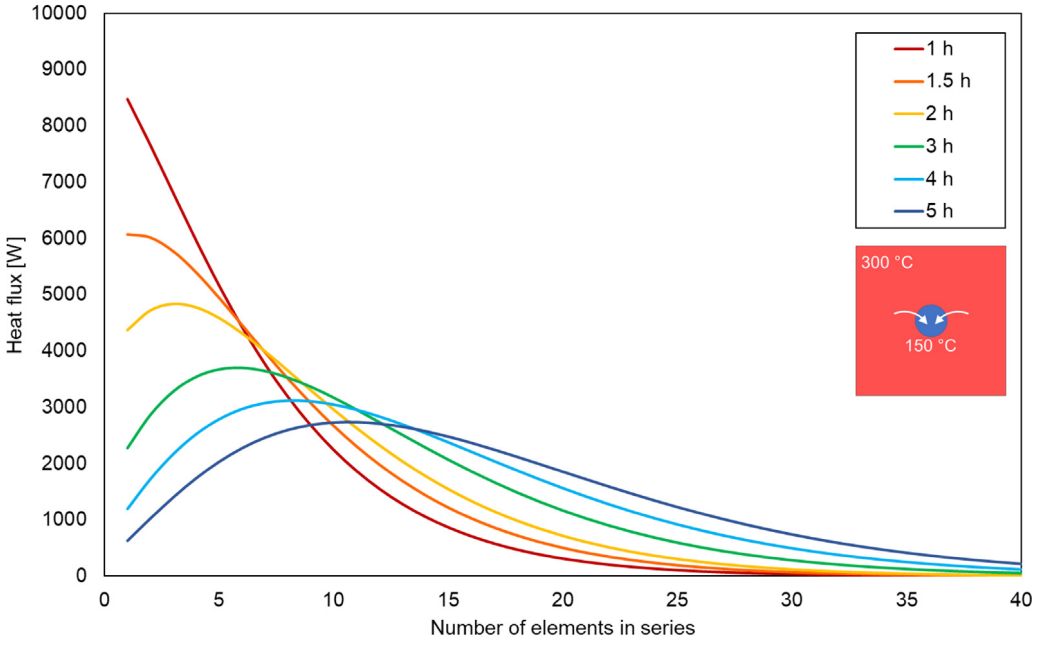

(b)

Fig. 8. Adiabatic analysis: oil heat fluxes at different hours for 44*2 configuration (500 kg/h, 5 bar) in charging (a) and discharging (b) (2 videos are available as additional files).

4.1.5. Oil heat fluxes over time

As already stated, the second configuration (44*2) has demonstrated the best overall performance in term of stored energy in reasonable time (5 h); for this reason, the oil heat flux at different time steps is plotted along the series, as shown in Fig. 8, for the charging phase (Fig. 8a) and the discharging one (Fig. 8b).

At the beginning of the simulation (i.e. 1 h), all the concrete blocks present the same temperature, thus the first one exchanges the maximum oil heat flux, as it can be seen from Fig. 8a. In charging phase, the oil cools down by flowing through the cold elements, and, consequently, the heat flux decreases through the series. Then, as the charging phase proceeds (i.e. 1.5, 2, 3 h, etc.), the first blocks asymptotically approaches the oil temperature and the heat flux sharply decreases to almost zero. The hot oil, which can be considered as a thermal wave, progressively reaches the following elements and the relative maximum heat flux moves to the central blocks and finally monotonically decreases as the oil temperature diminishes. The maximum value of heat flux moves gradually to the central blocks and reaches lower values.

During the discharging phase (Fig. 8b), the profiles are similar, but the oil and concrete temperatures are obviously switched.

Please cite this article as: L. Doretti, F. Martelletto and S. Mancin, Numerical analyses of concrete thermal energy storage systems: effect of the modules' arrangement. Energy Reports (2020), https://doi.org/10.1016/j.egyr.2020.07.002.

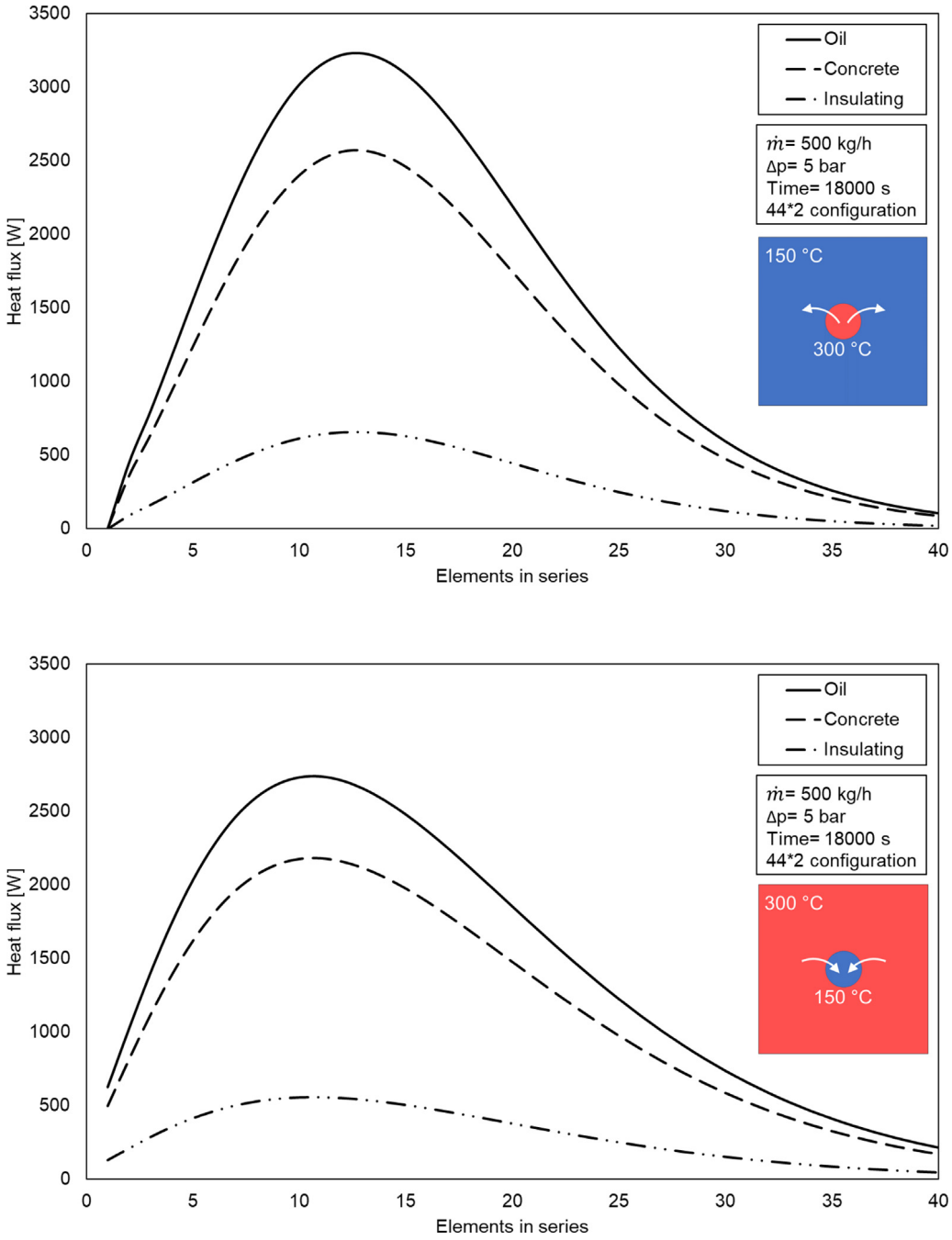

Fig. 9. Adiabatic analysis: heat fluxes at the end of the simulation for 44*2 configuration in charging (a) and discharging (b).

Hence, the oil becomes progressively hotter by flowing through the concrete blocks and this reduces the heat flux. Also, in this case, the curves present a maximum, but the profiles are smoother.

4.1.6. Heat fluxes along with the series

It is worth showing the profiles of the oil, concrete, insulating heat fluxes through the 44 elements of the 44*2 configuration after 5 h (i.e. at the end of the simulation) of both charging (Fig. 9a) and discharging (Fig. 9b).

Only three curves are shown because the reported simulation is carried out considering adiabatic conditions, so the loss heat flux is null and the difference between oil and concrete heat flux is equal to the insulating heat flux. They all have a maximum in the central blocks and then decreases progressively through the last element of the series. This means that the first blocks, have already exchanged heat with the oil mass flow rate in the previous hours, so the oil can reach the central block being still hot and charge the storage. This also means that even this configuration has not reached the maximum amount of storable energy.

4.2. Diabatic external boundaries

Further investigations can be made by introducing the heat flux between concrete blocks and the environment. The insulating

Please cite this article as: L. Doretti, F. Martelletto and S. Mancin, Numerical analyses of concrete thermal energy storage systems: effect of the modules' arrangement. Energy Reports (2020), https://doi.org/10.1016/j.egyr.2020.07.002.

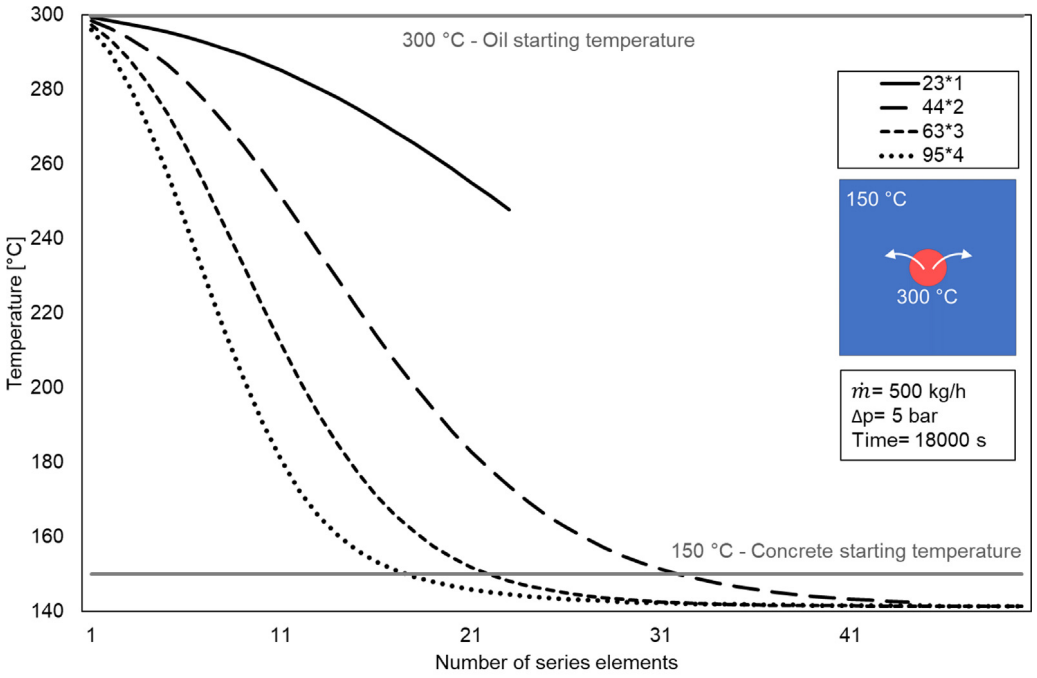

(a)

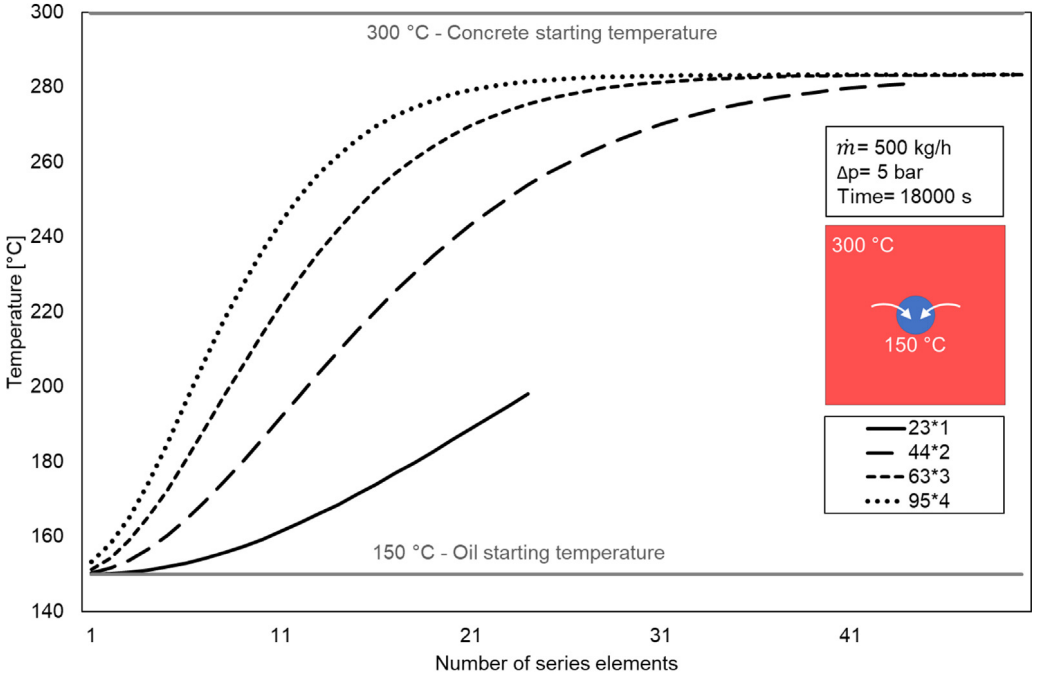

(b)

Fig. 10. Diabatic analysis: oil temperature at the end of the simulation in charging (a) and discharging (b) for different configurations.

materials exchange heat with the surrounding ambient, set at 20 °C. This new boundary condition remarkably affects the results of the simulations and the differences between the charging and discharging phases emerge, in terms of both temperature and exchanged heat. It is important to assess this condition because it seems closer to a real operating situation.

The exchanged thermal energy both in charging and discharging phases is reported in Tables 3–7 for the same combinations used for the previous analyses. In general, the results are similar to those obtained for adiabatic conditions, but there is important evidence: the asymptotic thermal energy related to charging and discharging set at different values and this is due to the loss of energy toward the environment. In fact, in charging phase, the concrete blocks are set at 150 °C and heated up by oil mass flow rate, which enters at 300 °C. Conversely, in discharging phase, the elements have 300 °C starting temperature, while the inlet oil one is equal to 150 °C. The environment temperature is always set at 20 °C, so the temperature difference between concrete and the surroundings changes during the simulation and it is different for the two phases. The diabatic boundary influences the heat flux

Please cite this article as: L. Doretti, F. Martelletto and S. Mancin, Numerical analyses of concrete thermal energy storage systems: effect of the modules' arrangement. Energy Reports (2020), https://doi.org/10.1016/j.egyr.2020.07.002.

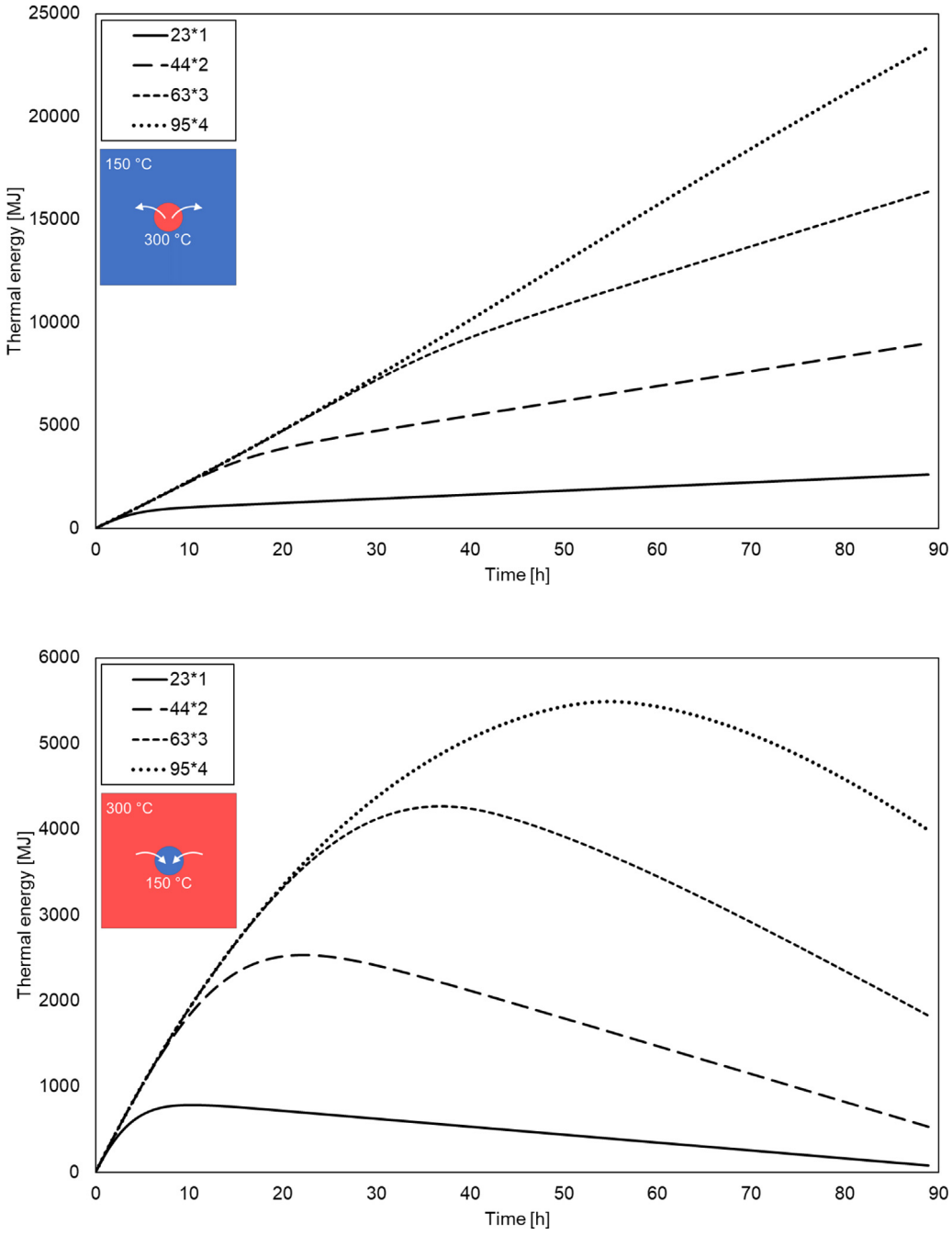

Fig. 11. Diabatic analysis: energy for different configurations at constant mass flow rate (500 kg/h) and pressure drop (5 bar) in charging (a) and discharging (b).

and the thermal energy too, specifically in the charging phase more amount of thermal energy is exchanged than in discharging.

4.2.1. Oil and concrete temperatures along with the series

The temperature curves at the end of the simulations, for different configurations, are reported even for the diabatic analyses in Fig. 10. As before, they are related to 500 kg/h oil mass flow rate and pressure drop of 5 bar. The general trend is similar to the adiabatic one and the second combination (44*2) is even in this condition the first that reaches the asymptotic value, both in the charging (Fig. 10a) and discharging phase (Fig. 10b).

Nevertheless, the two (44*2) asymptotes are set on different values compared with the adiabatic case. In the charging phase, the temperature profiles do not stop at 150 °C, which is the initial concrete one, but they reach 140 °C and this is due to the heat loss to the environment by the hot concrete modules. In fact, the blocks are cooled by the heat loss to the external ambient, so the oil is brought to that temperature, too. In the same way, in the discharging phase, the blocks initially are set at 300 °C and progressively decrease their temperature. The oil mass flow rate temperature cannot arise until 300 °C and stops at 287 °C. The temperature difference between the oil inlet and outlet is greater in charging than in the discharging phase. This causes a difference also in the related heat fluxes and thermal energy.

4.2.2. Thermal energy during time

The major differences can be highlighted considering the thermal energy during time, in Fig. 11. After the initial linear trend, the curves do not set on an asymptotic value, but there is an increase in charging and a decrease in the discharging phase. In

Please cite this article as: L. Doretti, F. Martelletto and S. Mancin, Numerical analyses of concrete thermal energy storage systems: effect of the modules' arrangement. Energy Reports (2020), https://doi.org/10.1016/j.egyr.2020.07.002.

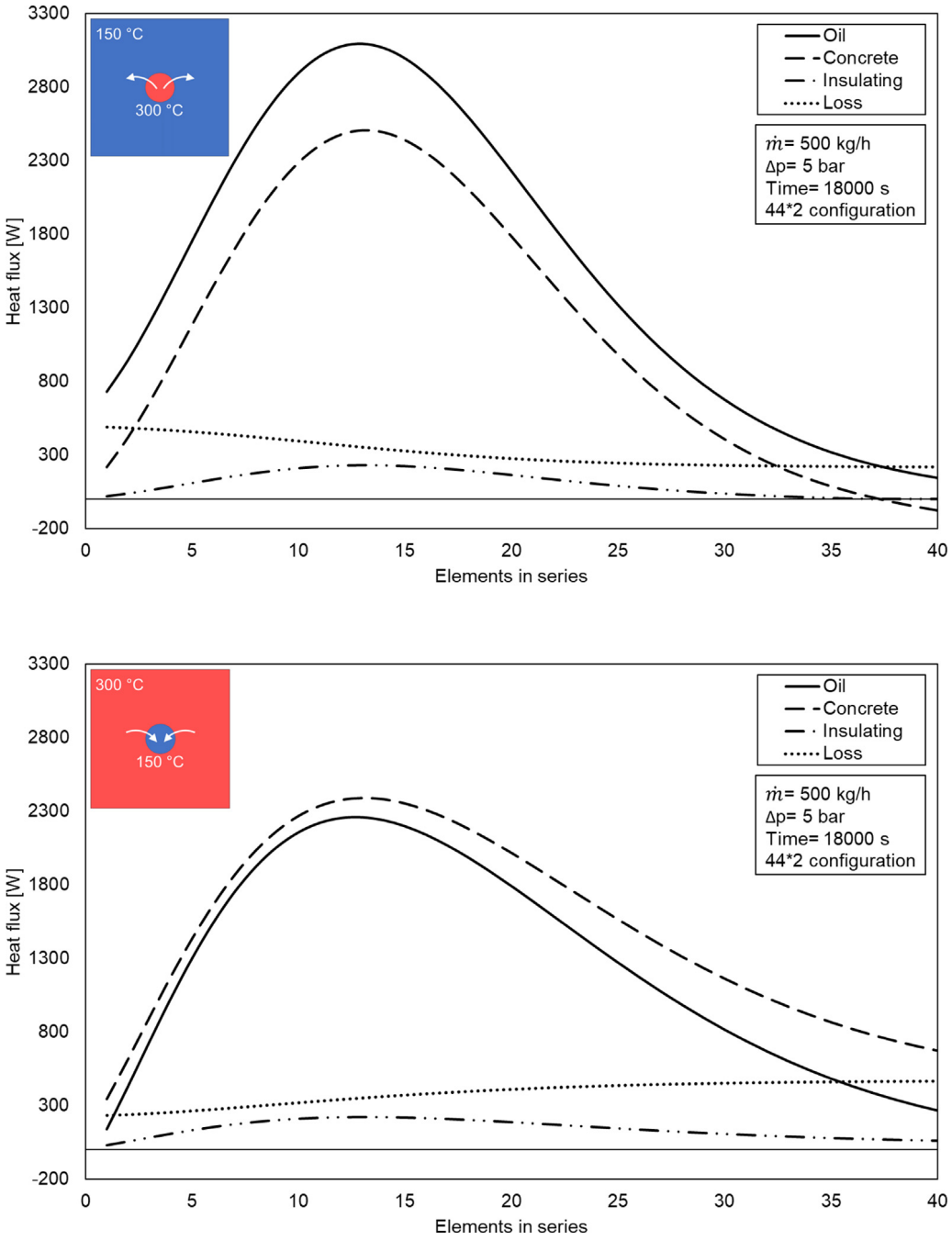

Fig. 12. Diabatic analysis: heat fluxes at the end of the simulation for 44*2 configuration in charging (a) and discharging (b).

the charging phase, the thermal energy keeps increasing, even if with a lower slope. In the discharging phase, instead, the thermal energy achieves a maximum, different for the various combinations, and then decreases progressively. It must be underlined that the two diagrams present different scales to improve the readability.

Even in diabatic conditions, the second combination (44*2) appears to be the optimum one in the range of operative time of a common CSP plant. It reaches the same thermal energy amount of the others, but with fewer concrete blocks.

4.2.3. Heat fluxes along with the series

The different heat fluxes at the end of the simulations (5 h) have been plotted along with the series even for this situation. There are some main changes compared to the adiabatic simulations; the results are reported in Fig. 12.

The loss heat flux has a relevant role in this situation, and it is more significant where the concrete block's temperature is higher. It happens for the first elements in charging phases, which have been already heated, and for the last ones in discharging phases, which still maintain a high temperature.

In the charging phase, the last elements encounter a negative concrete heat flux. This is due to the high loss heat flux, whose difference between the oil one brings the concrete heat flux below zero. For those elements, the insulating heat flux is null because it has already been balanced with the environment temperature, the central elements present the oil, concrete and insulating fluxes peaks.

In the discharging phase, the concrete heat flux has higher values that the oil one. Once again, this is due to the high loss heat

Please cite this article as: L. Doretti, F. Martelletto and S. Mancin, Numerical analyses of concrete thermal energy storage systems: effect of the modules' arrangement. Energy Reports (2020), https://doi.org/10.1016/j.egyr.2020.07.002.

flux, which enters in the balance and keeps the concrete heat flux higher than the oil one. The insulating heat flux has a peak in the middle, like the oil and concrete ones, while it is approximately negligible for the last blocks.

5. Conclusions

The numerical analysis for large-scale modularized concrete thermal energy storage systems was conducted. The simulations were carried out by means of a dedicated code, an improved version of the one proposed by Doretti et al. for single concrete TES block. Different arrangements of various elements in series, parallel and mixed configurations were investigated, and their performances compared, to determine the best configuration as a function of the imposed operating conditions.

The exchanged thermal energy was assessed both during the charging and discharging phase, considering adiabatic and diabatic external surfaces. The initial concrete, oil and environment temperatures were set at fixed values, to achieve comparable results. The oil mass flow rate, the pressure drops, and the process duration were instead varied to evaluate the performance of the different configurations. All the parameters were set to be suitable values for a real CSP plant.

At fixed total mass flow rate and pressure drop, the number of parallel branches was progressively increased. The number of elements in series for each branch was consequently calculated. The thermal energy increased at each consecutive branch, until an asymptotic value. For mass flow rate (500 kg/h) and pressure drop (5 bar), the most performant configuration was (44*2) that exchanged the same amount of energy of the following ones, but with fewer blocks. Hence, for the given operating conditions, the best possible configuration was found, considering thermal energy, pressure drops and economic issues.

The oil temperature profiles were also predicted and there are relevant differences between the adiabatic and the diabatic situations. In the adiabatic case, the curves tended with an asymptotic way to the starting concrete temperature, while in the diabatic case the heat loss shifted down them. The exchanged heat with the surroundings led to a progressive increase in the thermal energy in the charging phase while during the discharging phase a maximum value was observed. The best modules' configurations in diabatic conditions were the same for the adiabatic simulations but with different overall thermal energy, due to the heat loss to the surroundings.

Moreover, in the adiabatic case, after a few hours of operation, the exchanged heat fluxes presented a maximum in the central blocks of the series, the first elements had already been fully charged, so a peak appeared in the middle. In the diabatic case, the heat loss to the surroundings had a significant role and highlighted the differences between the charging and discharging phases. Its presence was not negligible and contributed to a more aware choice of the most suitable system.

CRediT authorship contribution statement

Luca Doretti: Conceptualization, Writing - original draft, Software. **Francesca Martelletto:** Conceptualization, Writing - original draft, Data curation. **Simone Mancin:** Conceptualization, Writing - review & editing, Validation.

Declaration of competing interest

The authors declare that they have no known competing financial interests or personal relationships that could have appeared to influence the work reported in this paper.

Acknowledgment

This work was partly supported by the University of Padova, Italy with project BIRD 2018 (Project number 188024 with title "*Modeling and multi-physics optimization of cellular solids for additive manufacturing in building applications*").

Appendix A. Supplementary data

Supplementary material related to this article can be found online at https://doi.org/10.1016/j.egyr.2020.07.002.

References

Achkari, O., El Fadar, A., 2020. Latest developments on TES and CSP technologies – Energy and environmental issues, applications and research trends. Appl. Therm. Eng. 167, 114806. http://dx.doi.org/10.1016/j.applthermaleng.2019.114806.

Amirifard, M., Kasaeian, A., Amidpour, M., 2018. Integration of a solar pond with a latent heat storage system. Renew. Energy 125, 682–693. http://dx.doi.org/10.1016/j.renene.2018.03.009.

Bergan, P.G., Greiner, C.J., 2014. A new type of large scale thermal energy storage. Energy Procedia 58, 152–159. http://dx.doi.org/10.1016/j.egypro.2014.10.422.

Besagni, G., Croci, L., 2019. Experimental study of a pilot-scale fin-and-tube phase change material storage. Appl. Therm. Eng. 160, 114089. http://dx.doi.org/10.1016/j.applthermaleng.2019.114089.

Cimmino, M., 2019. Semi-analytical method for g-function calculation of bore fields with series- and parallel-connected boreholes. Sci. Technol. Built Environ. 1–16. http://dx.doi.org/10.1080/23744731.2019.1622937.

Cocco, D., Migliari, L., Petrollese, M., 2016. A hybrid CSP–CPV system for improving the dispatchability of solar power plants. Energy Convers. Manage. 114, 312–323. http://dx.doi.org/10.1016/j.enconman.2016.02.015.

Cruickshank, C.A., Harrison, S.J., 2011. Thermal response of a series- and parallel-connected solar energy storage to multi-day charge sequences. Sol. Energy 85, 180–187. http://dx.doi.org/10.1016/j.solener.2010.09.010.

Dickinson, R.M., Cruickshank, C.A., Harrison, S.J., 2013. Charge and discharge strategies for a multi-tank thermal energy storage. Appl. Energy 109, 366–373. http://dx.doi.org/10.1016/j.apenergy.2012.11.032.

Dittus, F.W., Boelter, L.M.K., 1930. Heat transfer in automobile radiator of the tubular type. University of California at Berkley Publ. Eng. 2, 443–461.

Doretti, L., Martelletto, F., Mancin, S., 2019. A simplified analytical approach for concrete sensible thermal energy storages simulation. J. Energy Storage 22, 68–79. http://dx.doi.org/10.1016/j.est.2019.01.029.

Emam, M., Ahmed, M., 2018. Cooling concentrator photovoltaic systems using various configurations of phase change material heat sinks. Energy Convers. Manage. 158, 298–314. http://dx.doi.org/10.1016/j.enconman.2017.12.077.

Giannuzzi, G.M., Liberatore, R., Mele, D., Mazzucco, G., Xotta, G., Salomoni, V.A., Majorana, C.E., Di Maggio, R., 2017. Experimental campaign and numerical analyses of thermal storage concrete modules. Sol. Energy 157, 596–602. http://dx.doi.org/10.1016/j.solener.2017.08.041.

Gil, A., Medrano, M., Martorell, I., Làzaro, A., Dolado, P., Zalba, B., Cabeza, L.F., 2010. State of the art on high temperature thermal energy storage for power generation. Part 1 - Concepts, materials and modellization. Renew. Sustain. Energy Rev. 14, 31–55. http://dx.doi.org/10.1016/j.rser.2009.07.035.

Gnielinski, V., 2013. On heat transfer in tubes. Int. J. Heat Mass Transfer 63, 134–140. http://dx.doi.org/10.1016/j.ijheatmasstransfer.2013.04.015.

Haller, M.Y., Cruickshank, C.A., Streicher, W., Harrison, S.J., Andersen, E., Furbo, S., 2009. Methods to determine stratification efficiency of thermal energy storage processes – Review and theoretical comparison. Sol. Energy 83, 1847–1860. http://dx.doi.org/10.1016/j.solener.2009.06.019.

Herrmann, U., Kearney, D.W., 2002. Survey of thermal energy storage for parabolic trough power plants. J. Solar Energy Eng. 124 (2), 145–152. http://dx.doi.org/10.1115/1.1467601.

Hoivik, N., Greiner, C., Barragan, J., Crespo Iniesta, A., Skeie, G., Bergan, P., Blanco-Rodriguez, P., Calvet, N., 2019. Long-term performance results of concrete-based modular thermal energy storage system. J. Energy Storage 24, 100735. http://dx.doi.org/10.1016/j.est.2019.04.009.

Huang, H., Xiao, Y., Lin, J., Zhou, T., Liu, Y., Zhao, Q., 2020. Improvement of the efficiency of solar thermal energy storage systems by cascading a PCM unit with a water tank. J. Cleaner Prod. 245, 118864. http://dx.doi.org/10.1016/j.jclepro.2019.118864.

Keshavarz, A., Mehrabian, M.A., Abolghasemi, M., Mostafavi, A., 2010. A availability (exergy) analysis in a thermal energy storage system with the phase change materials arranged in series. Proc. IMechE 225 Part A: J. Power Energy 44–52. http://dx.doi.org/10.1177/09576509JPE1055.

Kuravi, S., Trahan, J., Goswami, D.Y., Rahman, M.M., Stefanakos, E.K., 2013. Thermal energy storage technologies and systems for concentrating solar power plants. Prog. Energy Combust. Sci. 39, 285–319. http://dx.doi.org/10.1016/j.pecs.2013.02.001.

Laing, D., Lehmann, D., Fiß, M., Bahl, C., 2009. Test results of concrete thermal energy storage for parabolic trough power plants. J. Sol. Energy Eng. 131, 041007–1–6. http://dx.doi.org/10.1115/1.3197844.

Laing, D., Steinmann, W.D., Tamme, R., Richter, C., 2006. Solid media thermal storage for parabolic trough power plants. Sol. Energy 80, 1283–1289. http://dx.doi.org/10.1016/j.solener.2006.06.003.

Macias, J.D., Gutierrez-Razo, R.A., Garcia-Lara, H.D., Cervantes-Alvarez, F., Bante-Guerra, J., Ares-Muzio, O., Romero-Paredes, H., Leon, N., Arancibia-Bulnes, C.A., Villafan-Vidales, H.I., Ramos-Sanchez, V., Alvarado-Gil, J.J., 2018. Thermal characterization of soda lime silicate glass-graphite composites for thermal energy storage. J. Renew. Sustain. Energy 10, 024701. http://dx.doi.org/10.1063/1.5003929.

Medrano, M., Gil, A., Martorell, I., Potau, X., Cabeza, L.F., 2010. State of the art on high-temperature thermal energy storage for power generation. Part 2 - Case studies. Renew. Sustain. Energy Rev. 14, 56–72. http://dx.doi.org/10.1016/j.rser.2009.07.036.

Paratherm NF Bulletin, available online in: http://paracalc.paratherm.com/ and http://www.paratherm.com/heat-transfer-fluids/paratherm-nf-heat-transfer-fluid/.

Pelay, U., Luo, L., Fan, Y., Stitou, D., Rood, M., 2017. Thermal energy storage systems for concentrated solar power plants. Renew. Sustain. Energy Rev. 79, 82–100. http://dx.doi.org/10.1016/j.rser.2017.03.139.

Rezaei, E., Barbato, M., Ortona, A., Haussener, S., 2020. Design and optimization of a high-temperature latent heat storage unit. Appl. Energy 261, 114330. http://dx.doi.org/10.1016/j.apenergy.2019.114330.

Rodat, S., Bruch, A., Dupassieux, N., El Mourchid, N., 2015. Unique Fresnel demonstrator including ORC and thermocline direct thermal storage: operating experience. Energy Procedia 69, 1667–1675. http://dx.doi.org/10.1016/j.egypro.2015.03.127.

Rodríguez, J.M., Sánchez, D., Martínez, G.S., Bennouna, E.G., Ikken, B., 2016. Techno-economic assessment of thermal energy storage solutions for a 1 MWe CSP-ORC power plant. Sol. Energy 140, 206–218. http://dx.doi.org/10.1016/j.solener.2016.11.007.

Rosato, A., Ciervo, A., Ciampi, G., Scorpio, M., Sibilio, S., 2019. Impact of seasonal thermal energy storage design on the dynamic performance of a solar heating system serving a small-scale Italian district composed of residential and school buildings. J. Energy Storage 25, 100889. http://dx.doi.org/10.1016/j.est.2019.100889.

Roy, S., Das, B., Biswas, A., Debnath, B.K., 2020. Energy and exergy analysis of a concrete-based thermal energy storage system. J. Inst. Eng. India Ser. C http://dx.doi.org/10.1007/s40032-020-00564-9.

Salomoni, V.A., Majorana, C.E., Giannuzzi, G.M., Miliozzi, A., Di Maggio, R., Girardi, F., Mele, D., Lucentini, M., 2014. Thermal storage of sensible heat using concrete modules in solar power plants. Sol. Energy 103, 303–315. http://dx.doi.org/10.1016/j.solener.2014.02.022.

Shang, B., Hu, J., Hu, R., Cheng, J., Luo, X., 2018. Modularized thermal storage unit of metal foam/paraffin composite. Int. J. Heat Mass Transfer 125, 596–603. http://dx.doi.org/10.1016/j.ijheatmasstransfer.2018.04.117.

Suárez, C., Pino, F.J., Guerra, J., 2020. A new simplified model for the unsteady response of concrete passive sensible TES systems. J. Energy Storage 27, 101042. http://dx.doi.org/10.1016/j.est.2019.101042.

Tamme, R., Laing, D., Steinmann, W.D., 2004. Advanced thermal energy storage technology for parabolic trough. J. Solar Energy Eng. 126, 794–800. http://dx.doi.org/10.1115/1.1687404.

Venegas-Reyes, E., Ortega-Avila, N., Rodríguez-Muñoz, N.A., Nájera-Trejo, M., Martín-Domínguez, I.R., Ibarra-Bahena, J., 2019. Parametric methodology to optimize the sizing of solar collector fields in series-parallel arrays. Processes 7, 294. http://dx.doi.org/10.3390/pr7050294.

Vigneshwaran, K., Singh Sodhi, G., Muthukumar, P., Subbiah, S., 2019. Concrete based high temperature thermal energy storage system: Experimental and numerical studies. Energy Convers. Manage. 198, 111905. http://dx.doi.org/10.1016/j.enconman.2019.111905.

Wu, M., Li, M., Xu, C., He, Y., Tao, W., 2014. The impact of concrete structure on the thermal performance of the dual-media thermocline thermal storage tank using concrete as the solid medium. Appl. Energy 113, 1363–1371. http://dx.doi.org/10.1016/j.apenergy.2013.08.044.

Yongtai, H., Lixian, X., Yaohua, Y., 2019. Study on design and thermal characteristics of vacuum tube solar collector intubated with heat storage tube. Int. J. Energy Res. 43 (13), 7409–7420. http://dx.doi.org/10.1002/er.4773.

Zhang, H.L., Baeyens, J., Degrève, J., Cacères, G., 2013. Concentrated solar power plants: Review and design methodology. Renew. Sustain. Energy Rev. 22, 466–481. http://dx.doi.org/10.1016/j.rser.2013.01.032.

Please cite this article as: L. Doretti, F. Martelletto and S. Mancin, Numerical analyses of concrete thermal energy storage systems: effect of the modules' arrangement. Energy Reports (2020), https://doi.org/10.1016/j.egyr.2020.07.002.